Chen-Hu, K., Garcia, M. J. F. G., Tonello, A. M. & Armada, A. G. (2021). Pilot Pouring in Superimposed Training for Channel Estimation in CB-FMT. *IEEE Transactions on Wireless Communications, 20*(6), pp. 3366–3380.

DOI: 10.1109/twc.2021.3049530

Pilot Pouring in Superimposed Training for Channel Estimation in CB-FMT

Kun Chen-Hu, *Member, IEEE,* M. Julia Fernández-Getino García, *Member, IEEE*, Andrea M. Tonello, *Senior Member, IEEE*, and Ana García Armada, *Senior Member, IEEE*

***Abstract*—Cyclic block filtered multi-tone (CB-FMT) is a waveform that can be efficiently synthesized through a filter-bank in the frequency domain. Although the main principles have been already established, channel estimation has not been addressed yet. This is because of assuming that the existing techniques based on pilot symbol assisted modulation (PSAM), implemented in OFDM-like schemes, can be reused. However, PSAM leads to an undesirable loss of data-rate. In this paper, an alternative method inspired by the superimposed training (ST) concept, namely pilot pouring ST (PPST), is proposed. In PPST, pilots are superimposed over data taking advantage of the particular spectral characteristics of CB-FMT. Exploiting the sub-channel spectrum, the pilot symbols are poured in those resources unused for data transmission. This spectral shaping of pilots is also exploited at the receiver to carry out channel estimation, by enhancing those channel estimates that exhibit a low data interference contribution. Furthermore, a frequency domain resource mapping strategy for the data and poured pilot symbols is proposed to enable an accurate estimation in strongly frequency-selective channels. The parameters of the proposed scheme are optimized to minimize the channel estimation mean squared error (MSE). Finally, several numerical results illustrate the performance advantages of the proposed technique as compared to other alternatives.**

***Index Terms*—5G, OFDM, SC-FDMA, CB-FMT, channel estimation, superimposed training, pilot pouring.**

I. Introduction

WAVEFORMS based on the filtered multi-tone (FMT) idea [1] have attracted the attention of the scientific community and industry in recent years. This interest is due to the fact that FMT has a better sub-channel frequency confinement provided by the use of prototype filters. Unlike for the well-known orthogonal frequency division multiplexing (OFDM) scheme [2], [3], either the out-of-band emissions can be reduced or the data-rate can be increased by using the same available frequency spectrum. In addition, FMT can be efficiently implemented with architectures based on poly-phase discrete Fourier transform (DFT) filter-banks [4]. There exist different multi-carrier waveforms proposed in the literature, such as filter-bank multi-carrier (FBMC) [5]–[7], universal filtered multi-carrier (UFMC) [8], [9], generalized frequency division multiplexing (GFDM) [10], [11] and cyclic block FMT (CB-FMT) [12], [13]. FBMC [5]–[7] is the waveform with the lowest out-out-band emissions due to the fact that each subcarrier is filtered by a well-localized prototype filter in the frequency domain. However, it possesses intrinsic inter-symbol and inter-carrier interferences (ISI and ICI), making even more complex the channel estimation and equalization processes. In UFMC [8], [9], a pulse shaping filter is applied to a group of conventional OFDM subcarriers. Its main drawback corresponds to the residual tail of the filter, which also provokes an intrinsic ISI and ICI. GFDM [10], [11] and CB-FMT [12], [13] are also block-filtered waveforms, similar to UFMC. However, they both exploit a circular pulse shaping that enables the use of the cyclic prefix (CP) and avoids the ISI and ICI due to multi-path channel. The main difference between these two waveforms is that the former is a non-orthogonal one, similar to FBMC and UFMC, while the latter is fully orthogonal, similar to OFDM. As a consequence of this orthogonality, CB-FMT allows a simple sub-channel pulse design and can reuse those channel estimation and equalization techniques designed for OFDM. Besides, it also exhibits a reduced peak-to-average power ratio (PAPR).

According to [13], the highly complex linear convolutions between data and prototype filters can be replaced in CB-FMT by a cyclic one at each sub-channel. This facilitates a block transmission and an efficient implementation of the convolution operation. It is carried out in the frequency domain via a concatenation of an inner (with respect to the channel) inverse DFT (IDFT), already implemented in OFDM, and a bank of outer DFTs, similarly to single-carrier frequency-division multiple access (SC-FDMA) [14], [15]. Therefore, a closer look at the CB-FMT scheme reveals that it can take advantage of the existing processing blocks of OFDM and/or SC-FDMA. Also, the filtering can be seen as an additional pre/post-coding operation, making it backward compatible to different communication standards based on OFDM, such as the Fourth and Fifth generation of mobile communication systems (4G and 5G) [14], [15].

Channel estimation and equalization are key aspects in the design of current and future communication systems. These tasks must be performed to fully exploit the benefits of many systems, such as reconfigurable intelligent surfaces [16] and communications at millimetre waves [17]. They must be ensured in an efficient way for the coherent detection of multi-carrier waveforms, where the effects introduced by the communication channel must be compensated before demodulation and symbol decision. Pilot symbol assisted modulation

Kun Chen-Hu, M. Julia Fernández-Getino García and Ana García Armada are with the Department of Signal Theory and Communications of Carlos III University of Madrid (Spain). E-mails: {kchen, mjulia, agarcia}@tsc.uc3m.es.

Andrea M. Tonello is with the Institute of Networked and Embedded Systems, University of Klagenfurt, Klagenfurt, Austria. E-mail: andrea.tonello@aau.at.

This work has been partially funded by project TERESA-ADA (TEC2017-90093-C3-2-R) (MINECO/AEI/FEDER, UE), and the work of A. M. Tonello has been supported in part by the Chair of Excellence Program of the Universidad Carlos III de Madrid.

(PSAM) [18] is the most widely employed technique for this purpose. In PSAM, several time-frequency resources are exclusively reserved for the transmission of pilot symbols, whose values are known by both ends of the communication link. At the receiver, the estimated channel at pilot positions can be obtained by typically applying a Least Squares (LS) criterion [19]. Finally, interpolation is required to obtain the estimated channel through the whole time-frequency resource grid. However, when the response of the multi-path channel is strongly frequency-selective and/or it suffers from a high Doppler effect, a significant amount of pilot symbols is required in order to track these time and frequency variations. This causes an important reduction of the effective data-rate. Besides, this disadvantage is even worse for those waveforms which rely on sub-channel processing, such as SC-FDMA, where the data of an entire sub-channel must be devoted to transmit the reference symbols. For example, in SC-FDMA waveform defined in both 4G [14] and 5G [15] standards, the sub-channel is always constrained to be twelve contiguous subcarriers, known as resource block (RB). In order to transmit the pilot symbols in a certain RB, all subcarriers of that RB are exclusively reserved for this purpose. In contrast, the channel estimation for OFDM in these standards may only require that one or two subcarriers are devoted for reference signals.

Alternatively, superimposed training (ST) [20]–[22] has been proposed in order to avoid the data-rate loss induced by PSAM. Since both data and pilot symbols are sharing the same available resources with different power values, data transmission is increased as compared to PSAM. However, this benefit comes at the expense of the pollution of the channel estimation by the interference generated by the superimposed data symbols. In order to improve the quality of the channel estimation, averaging in time and/or frequency dimensions is required. Finally, the superimposed pilot symbols must be subtracted from the signal before performing the demodulation and decision. Reference [20] proposed the combination of ST with OFDM, where data and pilot symbols simultaneously use all time-frequency resources, and the averaging process is only performed in the time dimension for several consecutive OFDM symbols. Additionally, this work showed that in the analysed cases the overall capacity of the system when using ST is higher than with PSAM. Reference [21] extended the ST technique to multiple antenna systems, where a low PAPR training sequence combined with different equalizers is proposed. Reference [22] exploited the ST technique not only for channel estimation, but also for multiple access. References [23], [24] combined ST with FBMC, where this combination has an even better performance as compared to the OFDM case given in [20]. Moreover, FBMC can take further advantage of the averaging process required by ST, due to the fact that its intrinsic data-interference produced by the loss of orthogonality can be also averaged out. Partial data ST (PDST) was proposed in [25], as a solution where only partial data is superimposed to pilot symbols at certain subcarriers, and it is capable of exploiting the advantages of both PSAM and ST. PDST is only applied to some specific resources, while the remaining ones are exclusively used for data symbol transmission. In order to avoid the error enhancement of the data placed in those resources with a superimposed pilot, coding was also considered.

To the best knowledge of the authors, channel estimation for CB-FMT has never been addressed before. Due to the fact that it is an orthogonal filter bank modulation, it has been assumed that it may reuse all techniques already designed for OFDM and/or SC-FDMA, and particularly those ones based on PSAM. However, a closer look shows that the combination of PSAM and CB-FMT is not the preferable choice. Similarly to SC-FDMA, CB-FMT is based on sub-channel processing. This imposes the use of a RB as a whole for pilot symbols, and consequently a high data-rate loss in practical implementations. On the other hand, the classical ST scheme cannot be directly applied to CB-FMT due to the fact that the allocated power to each sub-channel has not the same value, as a consequence of the filter shaping effect in the frequency domain. Hence, taking into account the power spectrum shape of CB-FMT and the benefits provided by PDST [25], we propose a novel concept denoted as pilot pouring ST (PPST). This proposal establishes a new generic framework for ST techniques, where the power of pilot symbols is determined depending on the amount of power allocated to data symbols at those time-frequency resources, which corresponds to a form of pilot pouring. At the receiver, a weighted average is proposed, where those pilot symbols containing a higher power contribute more to the channel estimation process. Furthermore, under high channel frequency selectivity, a dynamic resource mapping of both data and poured pilots over time is also proposed, in order to be able to effectively track the variations of the channel in the frequency domain.

The main contributions of this paper are summarized as follows:

- A Novel PPST channel estimation technique for CB-FMT is proposed. Our proposal brings a new framework to ST [20]. Herein, the allocated power to the pilot symbols at the transmitter is poured in the frequency domain by taking into account the shape of the sub-channel's frequency response. At the receiver, the use of an additional weighted average in the frequency domain is also proposed, which is capable of improving the channel estimates by selecting or weighing those pilot symbols with a higher allocated power. Unlike PSAM, it does not introduce any data-rate loss. Against ST, it does not decrease the power allocated to data symbols and the interference between data and pilots is reduced.
- To evaluate the performance of our proposal, the mean squared error (MSE) of the channel estimation is analysed. Moreover, the design of the pilot pouring and weighting coefficients is jointly carried out by minimizing the MSE.
- The use of dynamic resource mapping of both data and poured pilots over the time and frequency domain is also proposed. This is effective when the channel response is highly frequency-selective.
- The impact of the usage of PPST on the MSE, symbol error rate (SER) and achievable rate performance is evaluated numerically, showing the advantages of the

proposed approach.

The remainder of the paper is organized as follows. Section II introduces the system model of CB-FMT using a frequency domain low-complexity implementation. It is shown that the scheme can be interpreted as an OFDM with an additional transform carried out with a bank of outer FFTs and frequency domain filtering. Moreover, the channel effects and their estimation are also explained. Section III provides the description of our proposed PPST scheme for channel estimation in CB-FMT, and the analysis of its MSE. Section IV details some implementation remarks, such as the required signalling and a complexity comparison. Section V presents several numerical results for the proposed scheme under some realistic channel models, providing an assessment of the achieved system performance. Finally, in Section VI, the conclusions are reported.

II. System Model

The theoretical foundation of CB-FMT is summarized in this section. According to [13], the filter-bank can be efficiently implemented in the frequency domain, where the cyclic convolution is replaced by a dot product between data signals and the prototype pulse coefficients. As a consequence, CB-FMT can be synthesized by the existing well-known OFDM transceiver architecture and some pre/post-processing. Additionally, we also present the channel estimation and equalization techniques for CB-FMT that are inherited from OFDM.

A. CB-FMT

A single user system based on a CB-FMT waveform is considered. It is assumed that there is a base station (BS) which is serving a single user equipment (UE), and both of them can transmit and receive data symbols. The transmitter sends B contiguous CB-FMT symbols to the receiver, which are grouped in one slot. According to [12], the CB-FMT signal can be synthesized by using a circular convolution, instead of a linear one. The b-th CB-FMT symbol $x_b[n]$ is given by

$$x_b[n] = \frac{1}{\sqrt{K}} \sum_{k=0}^{K-1} \sum_{l=0}^{L-1} s_{b,k}[l]\, g_t\left[(n - lN_L)_M\right] \exp\left(j2\pi \frac{nk}{K}\right), \quad 0 \le n \le M-1, \quad 0 \le b \le B-1, \quad M = LN_L, \tag{1}$$

where M is the number of samples of one CB-FMT symbol, K corresponds to the number of sub-channels, L denotes the number of complex symbols transmitted at each sub-channel, $s_{b,k}[l]$ is the l-th complex symbol transmitted at the k-th sub-channel and b-th CB-FMT symbol, which belongs to a QAM constellation, and $g_t\left[(n)_M\right]$ denotes the cyclic repetition of the prototype synthesis pulse $g_t[n]$ with a period M. Note that $(n)_M$ is an abbreviation of $\mathrm{mod}(n, M)$, which is the integer modulo operator that provides the remainder of the ratio n/M.

The circular convolution can be also applied to the analysis filter-bank at the receiver. Assuming a distortion-free and noiseless channel, the output at the k-th sub-channel and b-th CB-FMT symbol is obtained as

$$z_{b,k}[l] = \frac{1}{\sqrt{K}} \sum_{n=0}^{M-1} y_b[n]\, g_r\left[(lN - n)_M\right] \exp\left(-j2\pi \frac{nk}{K}\right), \quad 0 \le k \le K-1, \quad 0 \le l \le L-1, \quad 0 \le b \le B-1, \tag{2}$$

where $y_b[n]$ is the input signal of the receiver for the b-th CB-FMT symbol and $g_r\left[(n)_M\right]$ is the periodic repetition of the prototype analysis pulse $g_r[n]$ with period M. Note that $y_b[n] = x_b[n]$ implies that $z_{b,k}[l] = s_{b,k}[l]$ with an orthogonal design of the cyclic filter bank.

B. Low-complexity frequency domain implementation

Reference [12] proposed the frequency domain implementation of CB-FMT. It reduces the complexity of both synthesis and analysis stages, especially regarding the filtering operation with respect to the conventional FMT scheme. This complexity reduction can be attained by exploiting the frequency domain, where the cyclic convolution can be replaced by a product.

Assuming that $M = LN_L = QK$, where Q is the number of non-zero coefficients of the frequency response of the prototype filter ($g_t[n]$), the M-point DFT of the transmitted signal obtained in (1) is given by

$$\begin{aligned} X_b[c] &= \sum_{n=0}^{M-1} x_b[n] \exp\left(-j2\pi \frac{cn}{M}\right) \\ &= \sum_{k=0}^{K-1} S_{b,k}[c - kQ]\, G_t[c - kQ], \end{aligned} \quad 0 \le c \le M-1, \quad 0 \le b \le B-1, \tag{3}$$

$$G_t[c] = \frac{1}{\sqrt{M}} \sum_{n=0}^{M-1} g_t[n] \exp\left(-j2\pi \frac{cn}{M}\right), \quad 0 \le c \le M-1, \tag{4}$$

$$S_{b,k}[c] = \frac{1}{\sqrt{L}} \sum_{l=0}^{L-1} s_{b,k}[l] \exp\left(-j2\pi \frac{cl}{L}\right), \quad 0 \le c \le M-1, \quad 0 \le b \le B-1, \tag{5}$$

where $G_t[c]$ is the frequency response of $g_t[n]$ (M-point DFT) and $S_{b,k}[c]$ corresponds to the L-point DFT of the data block $s_{b,k}[l]$. According to [12], [13], (3) can be rewritten as

$$X_b[c] = S_{b,k}[c - kQ]\, G_t[c - kQ], \quad 0 \le b \le B-1, \quad kQ \le c \le (k+1)Q - 1, \quad 0 \le k \le K-1, \tag{6}$$

due to the fact that $G_t[c] = 0$, $c \notin \{0, Q-1\}$.

Figure 1 summarizes the different blocks required for the efficient frequency domain implementation of CB-FMT at the transmitter, which consists in performing an L-point DFT (outer DFT) to data at each sub-channel, and cyclically extending them from L to Q points. Then, the sub-channel data are weighted by the Q coefficients of the prototype filter in the frequency domain. Finally, an M-point IDFT (inner IDFT) is applied to obtain the signal to be transmitted.

At the receiver, the analysis filter-bank can be implemented in the frequency domain too. From (2), the received signal

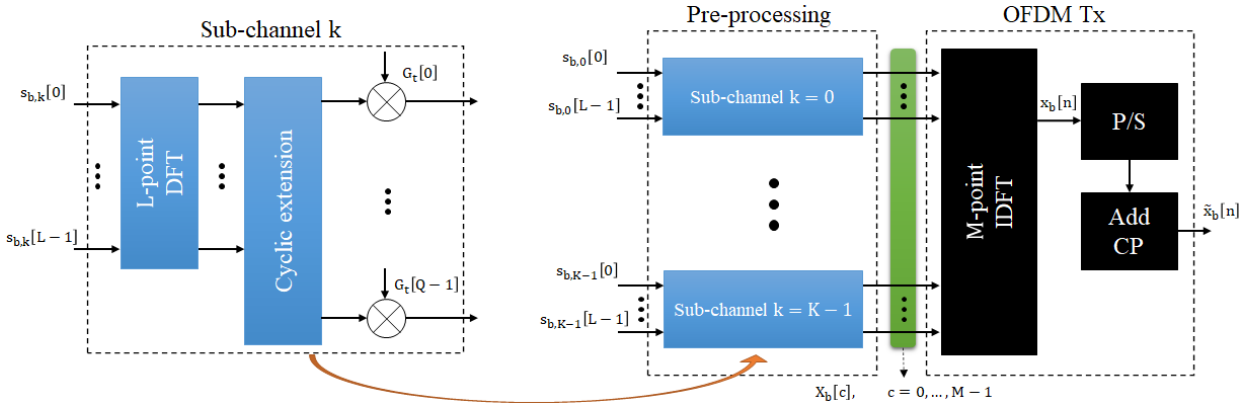

Fig. 1. Block diagram of the synthesis filter-bank of CB-FMT using the frequency domain implementation.

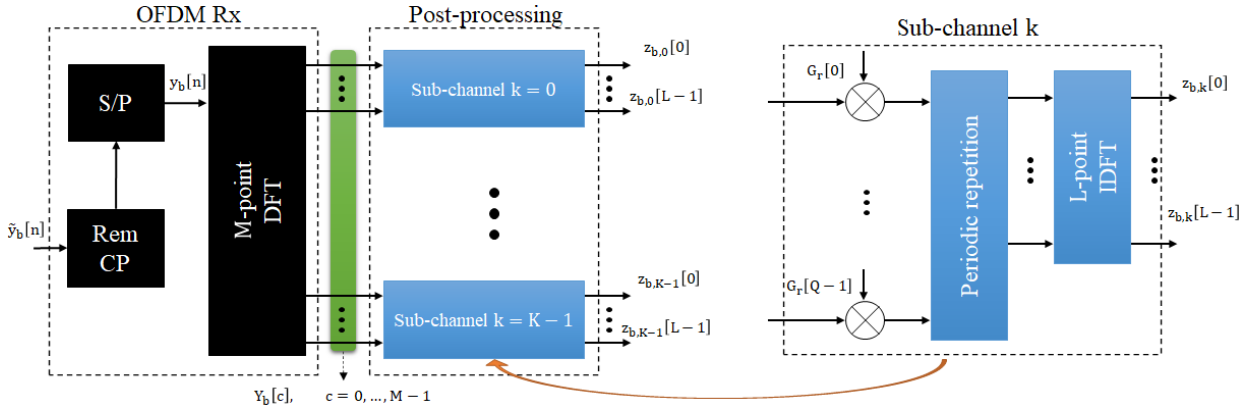

Fig. 2. Block diagram of the analysis filter-bank of CB-FMT using the frequency domain implementation.

$y_b\,[n]$ is substituted with the M-point IDFT of its frequency response, and hence, the following is obtained

$$z_{b,k}\,[l] = \sum_{c=0}^{M-1} Y_b\,[c + kQ]\,G_r\,[c] \exp\left(j2\pi \frac{cl}{L}\right), \qquad (7)$$

$$0 \le b \le B-1, \quad 0 \le k \le K-1, \quad 0 \le l \le L-1,$$

where $Y_b\,[c]$ and $G_r\,[c]$ are the frequency response of $y_b\,[n]$ and $g_r\,[n]$ (M-point DFT), respectively. Figure 2 summarizes the efficient implementation of CB-FMT at the receiver, where an inner M-point DFT is performed to the received data, and these results are weighted by the Q non-zero coefficients of the frequency response of the prototype pulse at each sub-channel. Then, a periodic repetition with period L is applied to every sub-channel, followed by an outer L-point IDFT.

From (6), we can see that the power of data symbols is shaped by the frequency response of the prototype filters, and hence, their average power can be obtained as

$$\mathbb{E}\left\{|X_b\,[c]|^2\right\} = |G_t\,[c - kQ]|^2, \quad 0 \le b \le B-1, \qquad (8)$$

$$kQ, \le c \le (k+1)Q - 1, \quad 0 \le k \le K-1,$$

where it has been assumed that the average power of complex data symbols is normalized to one. Figure 3 plots the spectrum of a CB-FMT signal, where it can be observed that each sub-channel is shaped by the prototype pulse in the frequency domain. Due to the use of a well-localized pulse in the frequency dimension, the out-of-band emission is effectively reduced. Moreover, as a consequence of this frequency confinement performed over each sub-channel, a portion of spectrum with very reduced power has appeared between contiguous sub-channels, which will be denoted as spectrum hole.

C. Comparison among CB-FMT, OFDM and SC-FDMA

Reference [12] highlighted that OFDM is a particular case of CB-FMT, where both schemes have an inner M-point IDFT/DFT in common described in (3). However, OFDM does neither require an outer L-point DFT/IDFT nor an additional filtering.

Hence, (4) and (5) should be substituted by $G_t\,[c] = 1$ and $S_{b,k}\,[c] = s_{b,k}\,[c]$ for $0 \le c \le M-1$, respectively.

Besides, SC-FDMA is a particular case of CB-FMT where the size of the outer DFT/IDFT is constrained to $L = 12$ when used in 4G and 5G standards, and the additional filtering is also removed ($G_t\,[c] = 1$ for $0 \le c \le M-1$).

D. Channel effects in CB-FMT

The backward compatibility feature of CB-FMT allows it to be straightforwardly implemented using an existing OFDM and/or SC-FDMA system (e.g. 4G and 5G), by adding some additional processing blocks at both transmitter and receiver. It also enables CB-FMT to obtain all the benefits of OFDM.

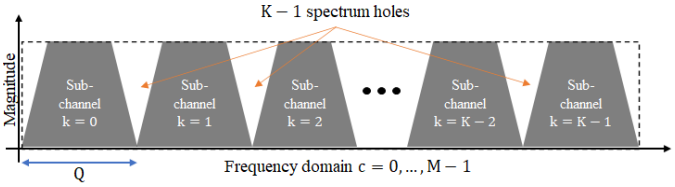

Fig. 3. The spectrum of CB-FMT shows that there is a spectrum hole between two contiguous sub-channels as a consequence of using well-localized prototype filters.

Firstly, CB-FMT will be able to avoid the ISI and ICI generated by the channel effects, by exploiting the well-known CP. Secondly, CB-FMT can take advantage of the channel estimation and equalization methods already developed for OFDM, which are techniques with an acceptable trade-off between complexity and performance. This advantage is not common to other FMT waveforms such as FBMC, UFMC and GFDM.

At the transmitter, after the inner M-point IDFT, a CP is appended to $x_b\,[n]$ given in (1) to build $\tilde{x}_b\,[n]$, $n = 0, \ldots, M + L_{CP} - 1$, where L_{CP} is the number of samples of the CP. Then, B CB-FMT symbols are serialized as

$$x\left[b\left(M + L_{CP}\right) + n\right] = \tilde{x}_b\,[n]\,, \tag{9}$$
$$0 \le b \le B-1, \quad 0 \le n \le M + L_{CP} - 1,$$

The signal $x\,[n]$, $0 \le n \le B\left(M + L_{CP}\right) - 1$, which corresponds to all samples in one slot, is digital-to-analogue converted and transmitted over the wireless channel. At the receiver, after analogue-to-digital conversion, the discrete time received signal is given as

$$y\,[n] = x\,[n] * h\,[n,\tau] + v\,[n]\,, \quad \tau = 0, \ldots, L_{CH} - 1, \tag{10}$$

where $v\,[n]$ corresponds to the additive white Gaussian noise (AWGN) which is distributed as $\mathcal{CN}(0, \sigma_v^2)$, $h\,[n,\tau]$ is the discrete time-varying channel impulse response and L_{CH} denotes the number of channel taps. Each tap is modelled as a complex random variable distributed as $\mathcal{CN}(0, \sigma_\tau^2)$. We assume that the channel gain is normalized as

$$\sum_{\tau=0}^{L_{CH}-1} \sigma_\tau^2 = 1, \tag{11}$$

and its suffers from a time variability with a channel correlation given by

$$\mathbb{E}\left\{\left|\left(h\,[n,\tau]\right)^* h\,[n+\Delta n,\tau]\right|\right\} = \left|J_0\left(2\pi f_d \Delta n\right)\right|, \tag{12}$$

where $f_d\,[Hz]$ is the Doppler frequency and $J_0\left(\cdot\right)$ is the zero-th order Bessel function of the first kind [26]. Moreover, in order to guarantee that the received signal is ISI and ICI free, it is assumed that the CP is long enough to mitigate the multi-path channel ($L_{CP} \ge L_{CH} - 1$) and the coherence time is sufficiently long to guarantee that the channel impulse response remains quasi-static for, at least, one CB-FMT symbol ($J_0\left(2\pi f_d\left(M + L_{CP}\right)\right) \approx 1$).

Then, assuming perfect time and frequency synchronization, $y\,[n]$ is separated into B CB-FMT symbols ($\tilde{y}_b\,[n]$, $0 \le b \le B-1$), the CP is removed to obtain $y_b\,[n]$, and its frequency response $Y_b\,[c]$ can be expressed as

$$Y_b\,[c] = H_b\,[c]\,X_b\,[c] + V_b\,[c]\,, \tag{13}$$
$$0 \le c \le M-1, \quad 0 \le b \le B-1,$$

where $H_b\,[c]$ and $V_b\,[c]$ are the channel's frequency response and noise, respectively, at the b-th CB-FMT symbol. Note that (13) corresponds to the well-known model consisting of M independent flat-fading channels as found in OFDM. These channels can be equalized by using the typical one-tap equalizer as

$$Y_b^{EQ}\,[c] = D_b\,[c]\left(H_b\,[c]\,X_b\,[c] + V_b\,[c]\right), \tag{14}$$
$$0 \le c \le M-1, \quad 0 \le b \le B-1,$$

where $D\,[c]$ is the post-equalizer coefficient. It is usually computed based on the zero-forcing (ZF) or minimum mean squared error (MMSE) criterion [27].

E. Channel estimation in multi-carrier waveforms

In order to perform the channel equalization defined in (14), the channel impulse response must be available for the computation of the equalizer ($D\,[c]$). Typically, many studies of multi-carrier waveforms assumed that either the channel estimation is perfect or the channel is estimated using the existing methods that were designed for OFDM. For the particular case of CB-FMT, all papers in the literature assume perfect channel estimation [4], [12], [13], without going into details on how it is obtained.

PSAM is the most frequently adopted channel estimation technique in different multi-carrier communication systems. Such is the case of 4G [14] and 5G [15], where some of the time-frequency resources are exclusively reserved to the transmission of pilot symbols, and others are dedicated to data. Due to the fact that CB-FMT is backward compatible with OFDM and SC-OFDM, it is straightforward to implement PSAM in CB-FMT following the same configuration of 4G and 5G standards, as described next. Let $\mathcal{A}$ denote the set of pairs of sub-channel and time indices as

$$\mathcal{A} = \left\{(k,b) \mid k \in \{0, \ldots, K-1\}, b \in \{0, \ldots B-1\}\right\}, \tag{15}$$

where its cardinality corresponds to $|\mathcal{A}| = K \times B$. Hence, $X_b\,[c]$ given in (6) can be split as

$$X_b\,[c] = \begin{cases} \text{data}, & (k,b) \in \mathcal{A}_d \\ \text{pilot}, & (k,b) \in \mathcal{A}_p \end{cases}, \quad kQ \le c \le (k+1)Q - 1, \tag{16}$$

where $\mathcal{A}_d$ and $\mathcal{A}_p$ are the subsets that contain the pairs of sub-channel and time indices for the data and pilot symbols, respectively, and their cardinalities are

$$\left|\mathcal{A}_p\right| = K^p \times B^p, \quad \left|\mathcal{A}_d\right| = (K \times B) - (K^p \times B^p)\,, \tag{17}$$

where K^p and B^p refer to the number of sub-channels and the number of CB-FMT symbols conveying pilot symbols, respectively. Equation (16) shows the inefficiency of PSAM in those waveforms based on sub-channel processing, where all subcarriers of one particular sub-channel of interest must

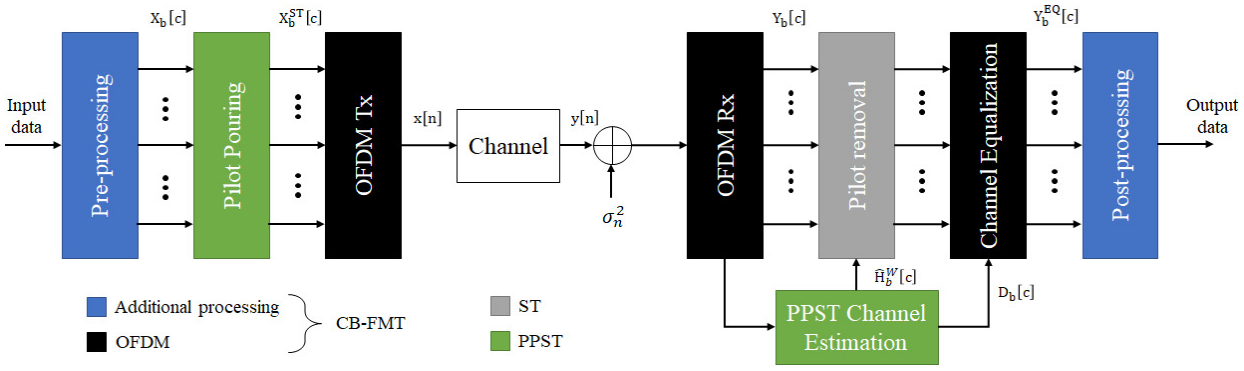

Fig. 4. Block diagram of CB-FMT based on frequency domain implementation with the proposed PPST for channel estimation (green), where the pilots are poured at the transmitter and the channel is estimated at the receiver.

be emptied of data in order to allow the transmission of pilot symbols. At the receiver, the channel is firstly estimated at the pilot positions in the time-frequency resource grid, where typically a LS method is applied. Then, the estimated channel is interpolated across both the time and frequency dimensions in order to obtain the channel estimates at the whole resource grid ($\mathcal{A}$). For the interpolation stage, the existing techniques in the literature [28], [29] are adopted. Details related to channel interpolation are not provided since this is out of the scope of this work.

On the other hand, ST has been proposed as an alternative to PSAM, since it is capable of maintaining the performance and reducing the overhead due to pilot symbols. ST assumes that the power is uniformly allocated to all subcarriers [20], [23], [24], and pilot symbols are superimposed to data ones in each resource. Hence, both of them have the same set of pairs of sub-channel and time indexes ($\mathcal{A}$). At the receiver, after performing the LS procedure, the channel estimates are averaged over the time and/or frequency dimensions in order to reduce the self-interference produced by data symbols and also noise effects. Then, a channel interpolation is required, similar to what is done in PSAM. Additionally, before performing the equalization, the superimposed pilot symbols must be removed from data. This ST technique cannot be straightforwardly applied to CB-FMT, because the power of each subcarrier is different due to the filtering process that is performed in order to reduce the out-of-band emissions.

Hence, the most straightforward way to obtain the channel estimates for CB-FMT consists in applying PSAM, as given by 4G [14] and 5G [15], due its similarity to OFDM and SC-FDMA. However, PSAM can be particularly inefficient for CB-FMT. In the next section, we propose a more efficient technique for this purpose based on the ST idea, adapted to the characteristics of this waveform.

III. Pilot Pouring Superimposed Training (PPST) for CB-FMT

In this section, the proposed channel estimation technique for CB-FMT, denoted as PPST, is described. According to [12] and as shown in Fig. 3, CB-FMT exhibits certain subcarrier frequencies where the power spectral density is very low, due to the use of the prototype filter at each sub-channel in order to provide a better frequency confinement. Consequently, the average power of the symbols placed at each subcarrier is directly shaped by the frequency response of this prototype filter as shown in (6), leading to some spectral holes at the edge bands of each sub-channel. Therefore, we propose the use of PPST as an alternative to the classical ST, where the power of the superimposed pilot symbols are adapted according to the frequency response of the prototype filter, taking advantage of the spectral shape of the signal. This will bring the advantage of much less interference between data and pilots. At the receiver, it is also described how to effectively perform an additional weighted average at each sub-channel in order to further mitigate the data-interference during channel training. The optimum values for the pilot pouring and weighted average coefficients are obtained with the criterion of minimizing the MSE of channel estimation, which is analytically derived. Finally, it is described how to map data and pilot symbols over the spectrum for the case of highly frequency-selective channels, to effectively track the selectivity of the channel in the frequency dimension.

Figure 4 plots the block diagram of CB-FMT based on OFDM with the proposed PPST. At the transmitter, the pilot symbols are poured into the output signal of the pre-processing block, and hence, the superimposed data and pilot symbols are transmitted by using the well-known OFDM transceiver. At the receiver, we perform the PPST channel estimation at the output of the OFDM block. Then, the superimposed pilot symbols are removed, in a similar manner as the classical ST, and they are post-equalized. Finally, a post-processing is required to recover the transmitted complex symbols.

A. Pilot pouring at the transmitter

At the transmitter, data and pilot symbols are summed up to build $X_b^{ST}[c]$ which is given by

$$X_b^{ST}[c] = X_b[c] + W^T[c]\, X_b^p[c], \tag{18}$$

$$0 \le c \le M-1, \quad 0 \le b \le B-1,$$

where $X_b^p[c]$ is the pilot symbol, $W^T[c]$ denotes the pilot amplitude allocation coefficient and $X_b[c]$ corresponds to the

data symbols given in (6) at the c-th subcarrier and b-th CB-FMT symbol. It is assumed that the power of the pilot symbols is also normalized to one. Besides, $W^T[c]$ is constrained to

$$W^T[c] = 0, \quad c < \frac{Q}{2} \quad \text{or} \quad c \geq M - \frac{Q}{2}, \tag{19}$$

in order to avoid the superposition of pilot symbols at both edges of the band. In this way, the low out-of-band emissions feature of CB-FMT is kept unaltered. Additionally, note that the focus in this work is on the amplitude of the pilot pouring coefficients ($W^T[c]$), while the phase component has not got any restriction and could be adjusted to take into account other requirements.

Considering (8), it is proposed not to uniformly allocate the power to the ST pilot symbols in the spectrum. In turn, the ST pilot symbols power is poured according to the power spectrum of the transmit prototype pulse and, in particular, pouring more power into the existing data spectrum holes. The values for $W^T[c]$ that yield an accurate channel estimation are determined by the optimization problem described in Subsection III-C.

B. Channel estimation at the receiver

At the receiver, following (13), the signal at the output of the inner DFT can be modelled as

$$\begin{aligned} Y_b[c] &= H_b[c] X_b^{ST}[c] + V_b[c] \\ &= H_b[c] \left(X_b[c] + W^T[c] X_b^p[c] \right) + V_b[c], \\ & 0 \leq c \leq M-1, \quad 0 \leq b \leq B-1. \end{aligned} \tag{20}$$

Applying the LS criterion to (20), the estimated channel for each time-frequency resource can be obtained as

$$\begin{aligned} \widehat{H}_b[c] &= \frac{Y_b[c]}{W^T[c] X_b^p[c]} \\ &= H_b[c] \left(1 + \frac{X_b[c]}{W^T[c] X_b^p[c]} \right) + \frac{V_b[c]}{W^T[c] X_b^p[c]}, \\ & 0 \leq c \leq M-1, \quad 0 \leq b \leq B-1. \end{aligned} \tag{21}$$

According to [20], [24], [25], an arithmetic average is a must for channel estimation techniques based on classical ST. In this way, several contiguous time-frequency resources of the grid are averaged in order to reduce the effect of noise and cancel self-interference generated by data symbols, as far as possible. Note that this operation requires that the channel's frequency response remains quasi-static for all time-frequency resources to be averaged. Hence, we firstly propose to perform an arithmetic average over the B CB-FMT symbols (time dimension) as

$$\begin{aligned} \widehat{H}[c] &= H[c] + \\ &+ \frac{1}{B} \frac{1}{W^T[c]} \left(H[c] \sum_{b=0}^{B-1} \frac{X_b[c]}{X_b^p[c]} + \sum_{b=0}^{B-1} \frac{V_b[c]}{X_b^p[c]} \right), \\ & 0 \leq c \leq M-1, \end{aligned} \tag{22}$$

where it has been assumed that the coherence time of the channel impulse response is at least equal to the duration of one slot

$$H[c] = H_b[c], \quad 0 \leq b \leq B-1, \quad 0 \leq c \leq M-1, \tag{23}$$

and the corresponding MSE of the channel estimation at the c-th subcarrier is given by

$$\begin{aligned} \text{MSE}_c &= \frac{|G_t[c - kQ]|^2 + \sigma_v^2}{B \left| W^T[c] \right|^2}, \\ & kQ \leq c \leq (k+1)Q - 1, \quad 0 \leq k \leq K-1, \end{aligned} \tag{24}$$

whose derivation is detailed in Appendix A. It can be seen that the quality of the channel estimates is not the same for all subcarriers. It depends on the frequency response of the prototype filter used at the transmitter and the power of the poured pilot symbols. Note that, the MSE of classical ST [20] is a particular case of (22), where the pilot pouring coefficients ($W[c]$) and the frequency response of the prototype filter ($G_t[c]$) have the same value for any subcarrier.

Taking into account (22), $\widehat{H}[c]$ cannot be directly employed for the computation of equalizers $D[c]$, due to the fact that the channel estimates corresponding to the mid band at each sub-channel suffer a high MSE, and thus, the performance of the system would be significantly degraded. In order to obtain a more accurate channel estimation and improve the performance of the equalizers, an additional weighted average in the frequency domain for each spectrum hole is proposed (see Fig. 5), where the estimated channel at each subcarrier, obtained in (22), is weighted by $W^R[c]$, $0 \leq c \leq M-1$ as

$$\widehat{H}^W[k] = \sum_{c \in \mathcal{H}_k} W^R[c] \widehat{H}[c], \quad 0 \leq k \leq K-2, \tag{25}$$

$$0 < W^R[c] < 1, \quad \sum_{c \in \mathcal{H}_k} W^R[c] = 1, \quad 0 \leq k \leq K-2, \tag{26}$$

$$\mathcal{H}_k = \{kQ, \ldots (k+1)Q - 1\} + \frac{Q}{2}, \tag{27}$$

where the set $\mathcal{H}_k$ denotes the sub-carrier indexes corresponding to the k-th spectrum hole, and it is assumed that the channel's frequency response remains flat at each spectrum hole as

$$H[c_i] = H\left[c_j\right], \quad c_i \neq c_j, \quad \forall c_i, c_j \in \mathcal{H}_k. \tag{28}$$

Hence, the MSE of the channel estimation performed in the k-th spectrum hole after the weighted average is given by

$$\begin{aligned} \text{MSE}_k &= \sum_{c \in \mathcal{H}_k} \left(W^R[c] \right)^2 \text{MSE}_c \\ &= \sum_{c \in \mathcal{H}_k} \left(W^R[c] \right)^2 \frac{\left| G_t\left[(c - kQ)_Q\right] \right|^2 + \sigma_v^2}{B \left| W^T[c] \right|^2}, \\ & 0 \leq k \leq K-2, \end{aligned} \tag{29}$$

where the fact that data and pilot symbols and noise are uncorrelated random variables among different subcarriers is considered. The values of the weighted average coefficients to minimize the MSE are determined in Subsection III-C.

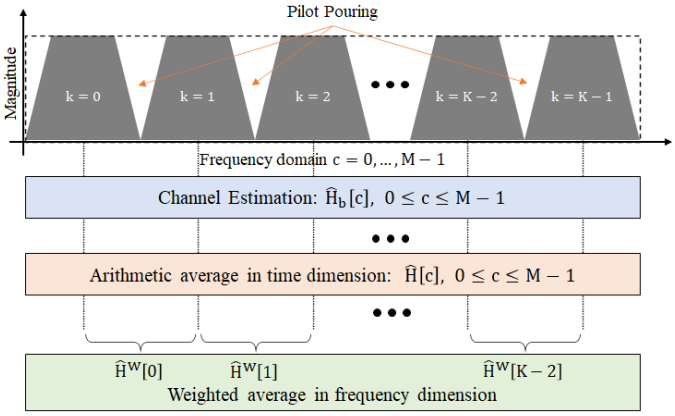

Fig. 5. Example of pilot pouring into the $K-1$ spectrum holes at the transmitter, and the channel estimation based on both arithmetic and weighted averages at the receiver.

C. Minimization of the MSE of the channel estimation

The optimum power allocation for the pilot pouring and the weighted average coefficients in the frequency domain can be obtained by minimizing the MSE given in (29). Without loss of generality and for the sake of notation, we describe the optimization problem for one particular spectrum hole of interest ($\forall\ k \in \{0,\ldots,K-2\}$) as

$$\begin{aligned} \min_{\substack{|W^T[c]|^2 \\ W^R[c] \\ c\in\mathcal{H}_k}} \quad & \sum_{c\in\mathcal{H}_k} \frac{\left(W^R[c]\right)^2}{\left|W^T[c]\right|^2}\left(\left|G_t\left[(c-kQ)_Q\right]\right|^2+\sigma_v^2\right), \\ \text{s.t.} \quad & 0<W^R[c]<1, \quad \sum_{c\in\mathcal{H}_k} W^R[c]=1, \\ & 0<\left|W^T[c]\right|^2\le\eta^2. \end{aligned} \tag{30}$$

where η^2 denotes the maximum allowed power per subcarrier and it is obtained as

$$\eta^2=\max_c\left\{\left|G_t[c]\right|^2\right\}, \quad 0\le c\le M-1. \tag{31}$$

According to [30], the optimization problem described in (30) is strictly convex with respect to $W^R[c]$ and quasi-convex with respect to $\left|W^T[c]\right|^2$. The former is due to the fact that it is the well-known square function, while the latter is due to the existence of poles in the function. However, given the restriction of $0<\left|W^T[c]\right|^2\le\eta^2$, all the poles can be avoided and (30) is also convex with respect to the pilot pouring coefficients. Hence, it is possible to obtain $W^T_{\text{opt}}[c]$ and $W^R_{\text{opt}}[c]$ that guarantee the minimum value of MSE of the channel estimation. Typically, the pilot pouring and weighted average coefficients can be efficiently determined by using the well-known bisection method [31].

Inspecting (24)-(30), the optimization problem will jointly decide the parameters to be used at both transmitter and receiver sides to reduce the MSE. At the transmitter, it will allocate more power to the pilot symbols placed at spectrum holes of the CB-FMT signal. Consequently, the MSE at these spectrum holes will be low, not only due to high power of the poured pilot symbols ($W_t[c]\uparrow$ at the denominator of (24)), but also because the spectrum holes only experience a very low data interference ($G_t[c]\downarrow$ at the numerator of (24)). Then, at the receiver, the coefficients of the weighted average ($W_r[c]$) will select/enhance those channel estimates obtained at the spectrum holes, which correspond to those with a low MSE.

Furthermore, note that our proposed pilot pouring technique at the transmitter can be applied to any multi-carrier waveform that does not exhibit a uniform power among subcarriers, such as UFMC and GFDM. However, these non-orthogonal waveforms require an additional processing to obtain accurate-enough channel estimates, due to the presence of intrinsic ISI and ICI.

D. Channel estimation for strongly frequency-selective channels

In the previous subsections, it was assumed that the channel's frequency response remains flat for each sub-channel of the CB-FMT signal (see (28)), in order to be able to perform a weighted average in the frequency domain. However, when the channel is strongly frequency-selective, the quality of the channel estimates after the weighted average may be seriously compromised.

In order to effectively estimate the frequency-selective channel in the frequency domain, the distance of any two contiguous spectrum holes should be decreased. This corresponds to a reduction of the bandwidth of the prototype filter ($Q\downarrow$) and an increase on the number of sub-channels ($K\uparrow$), to obtain more channel estimates in the frequency domain ($\widehat{H}^W[k]$, $0\le k\le K-2$). Moreover, it is also proposed to shift the sub-channels in the frequency domain at each new CB-FMT symbol transmission, and therefore, the spectrum holes are placed at different subcarriers in each consecutive CB-FMT symbol. At the receiver, the channel estimation at each spectrum hole for every CB-FMT symbol is obtained, and those estimates from different CB-FMT symbols are merged to obtain $\widehat{H}^W[k]$.

The B CB-FMT symbols in one slot are split into N_F sub-slots consisting of F CB-FMT symbols each ($B=N_F F$). At the transmitter, after the pilot pouring block, the data with the superimposed pilot symbols are frequency shifted as

$$\begin{aligned} \tilde{X}_b^{ST}\left[c+f\frac{Q}{F}\right]=X_b^{ST}[c], \quad f=\text{mod}(b,F), \\ 0\le c\le M-1, \quad 0\le b\le B-1, \end{aligned} \tag{32}$$

where it is ensured that the fraction between Q and F is an integer number by design. Note that the frequency shift pattern performed at the F CB-FMT symbols of one sub-slot is repeated for the N_F sub-slots. Then, $\tilde{X}_b^{ST}[c]$ is fed to the M-point IDFT and transmitted.

At the receiver, from (21), the channel estimates for each CB-FMT symbol ($\widehat{H}_b[c]$, $0\le b\le B-1$) are obtained. However, the arithmetic average in the time dimension is only performed in those CB-FMT symbols that have the same frequency shift pattern as

$$\widehat{H}_f[c]=\frac{1}{N_F}\sum_{b\in\mathcal{B}_f}\widehat{H}_b[c], \quad 0\le f\le F-1, \tag{33}$$

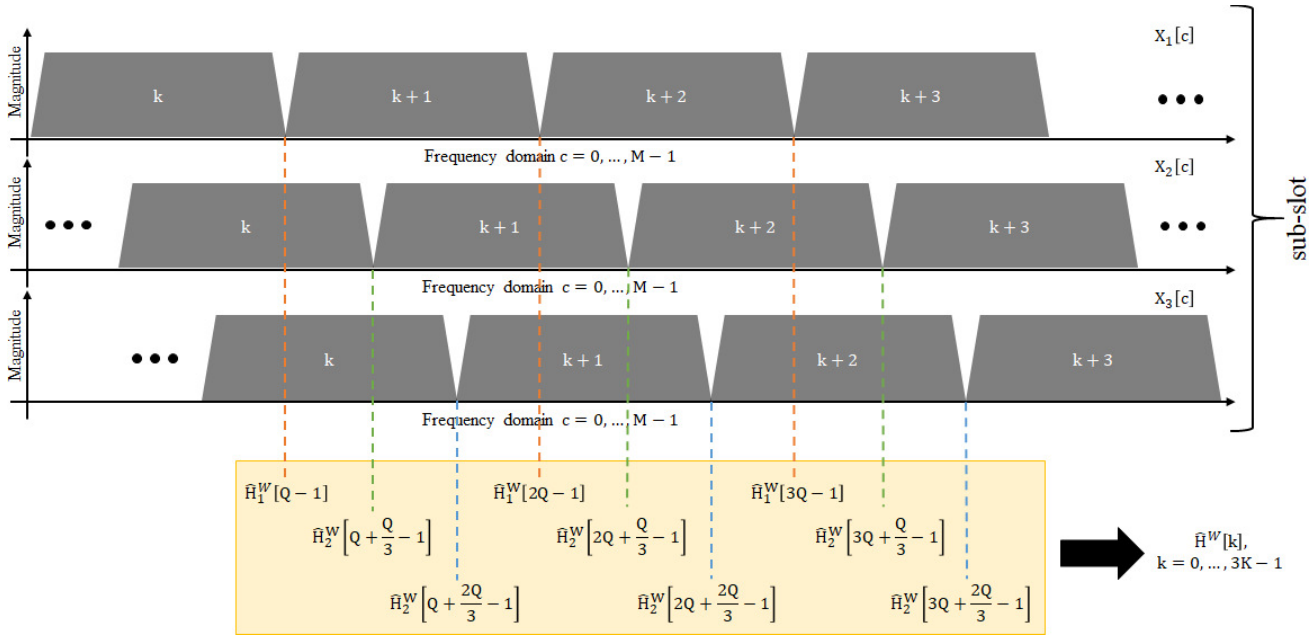

Fig. 6. Channel estimation for strongly frequency-selective channels when $F = 3$, where the spectrum holes and their corresponding poured pilots are shifted in the frequency dimension for each CB-FMT symbol at the transmitter. Then, accurate channel estimates can be obtained at different subcarriers at the receiver.

$$\mathcal{B}_f = \{iF + f \mid 0 \leq i \leq N_F - 1\}, \quad 0 \leq c \leq M - 1, \quad (34)$$

where the set $\mathcal{B}_f$ provides the indexes that correspond to the f-th CB-FMT symbol of each sub-slot. Then, a weighted average over the frequency dimensions is performed as,

$$\widehat{H}_f^W[k] = \sum_{c \in \mathcal{H}_{k,f}} W^R[c]\, \widehat{H}_f[c], \quad 0 \leq k \leq K - 2, \quad (35)$$

$$0 < W^R[c] < 1, \quad \sum_{c \in \mathcal{H}_{k,f}} W^R[c] = 1, \quad 0 \leq k \leq K-2, \quad (36)$$

$$\mathcal{H}_{k,f} = \{kQ, \ldots (k+1)Q - 1\} + \frac{Q}{2} + f\frac{Q}{F}, \quad (37)$$

where the new set $\mathcal{H}_{k,f}$ takes into account that each CB-FMT symbol of the sub-slot has a different frequency shift.

Finally, the channel estimates from different CB-FMT symbols are merged as

$$\widehat{H}[kF + f] = \widehat{H}_f[k], \quad 0 \leq k \leq K - 2, \quad 0 \leq f \leq F - 1. \quad (38)$$

Figure 6 plots a practical example of PPST designed for a frequency-selective channel, for the particular case of $F = 3$. At the transmitter, the spectrum holes are placed at different subcarriers, covering the whole signal band. At the receiver, after performing the LS procedure to obtain the channel estimates and the arithmetic average (time) and weighted average (frequency), one channel estimate per spectrum hole is attained. Finally, the improved channel estimation is obtained by merging the different channel estimates from the $F = 3$ CB-FMT symbols.

IV. Implementation Remarks

In this section, it will be detailed how to implement our proposed PPST in a realistic link, taking into account the required signalling and the additional complexity when compared to the traditional PSAM technique.

A. Signalling

In order to perform our proposed PPST, the parameters $W^T[c]$ and $W^R[c]$ must be obtained and shared between the BS and the UE before data transmission. In Fig. 7, this signalling process is detailed. The UE transmits a synchronization frame in order to let the BS estimate the SNR and perform time and frequency synchronization, which are required in any system. For our particular case of PPST, according to (30), the pilot pouring and weighted average coefficients can be obtained by the BS according to the estimated noise power (σ_v^2), the selected filter $G_t[c]$ and bandwidth of the prototype filter (Q), which are design choices known beforehand by both entities. Then, these parameters are reported to the UE, and hence, both entities can transmit their data frames using PPST. Furthermore, these parameters may be changed during the transmission. In such case, either the UE may send a request for new parameters or the BS may directly update them.

We can see that the additional overhead induced by reporting the pilot pouring and weighted average coefficients is negligible when compared to the amount of transmitted data rate. Besides, in order to further reduce this overhead, a set of $W^T[c]$ and $W^R[c]$ may be previously computed and stored in memory (offline mode) for different values of noise power (σ_v^2) and for some chosen prototype filters. These different sets may be also tagged with an index to ease their identification. During the phase of sharing or updating, only these indexes should be exchanged, reducing overhead.

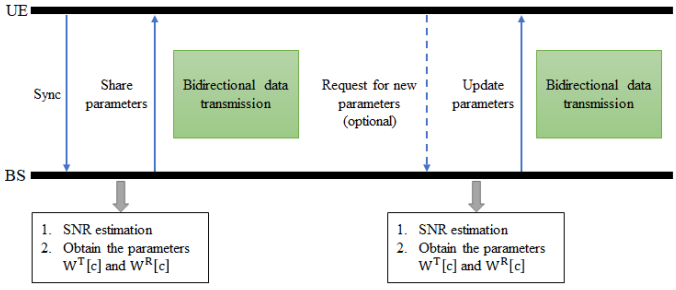

Fig. 7. Signalling in PPST to exchange the pilot pouring and weighted average coefficients.

B. Complexity

The additional complexity required by PPST proposal, as compared to PSAM, mainly corresponds to the solution of optimization problem described in (30) in order to obtain the pilot pouring and weighted average coefficients. According to [31], the complexity of the bisection method can be estimated by the number of iterations required to achieve a given error or tolerance ($I(\epsilon)$). Hence, performing some straightforward manipulations and assuming that all sub-channels use the same prototype filter, the number of required iterations for (30) is

$$I(\epsilon) = Q\left(I^T(\epsilon) \times I^R(\epsilon)\right) \geq Q\left(\log_2\left(\frac{\eta}{\epsilon}\right) \times \log_2\left(\frac{1}{\epsilon}\right)\right), \tag{39}$$

where $I^T(\epsilon)$ and $I^R(\epsilon)$ are the estimated number of iterations for the pilot pouring and weighted average coefficients, respectively.

Given these coefficients, they are exploited in data transmission, and hence, an additional number of operations is required to configure the transmitted waveform in comparison to PSAM. At the transmitter, the pilot pouring corresponds to a power scaling required in any communication system. Instead of multiplying by the same scaling factor to all subcarriers as in PSAM, each subcarrier has a different value. However, there is no increase in the number of required products. At the receiver, our proposal requires a weighted average which involves $2M$ additional real products and sums for each CB-FMT symbol.

V. Performance Evaluation

In this section, several numerical results are provided in order to show the performance of the proposed PPST technique for channel estimation as compared to traditional PSAM, when both schemes are implemented in CB-FMT.

A summary of the simulation parameters is given in Table I. The channel model adopted for the simulation corresponds to the tapped delay line (TDL) model proposed by the 3GPP to evaluate 5G performance [32]. In order to show the benefit of our proposal, PSAM technique (16) is set as the reference case to be compared with, making use of the demodulation reference signals (DM-RS) given in 5G [15]. Specifically, the configuration Type 1 (C1) pilot pattern is chosen for the frequency domain, while for the time dimension the number of chosen multi-carrier symbols depends on the Doppler frequency [33]. In our particular case, one and two multi-carrier symbols out of every fourteen were chosen for $f_d = 35$ Hz and $f_d = 300$ Hz, respectively (denoted as 5G-C1-1 and 5G-C1-2).

TABLE I
Simulation Parameters

M	1024	**Interp. Method**	Cubic
L	12, 24 & 36	**Delay Spread**	39 & 634 ns
Q	16, 28 & 38	$\mathbf{f_d}$	35 & 300 Hz
B	1, 4 & 6	**Equalization**	MMSE
F	2 & 3	**Δf**	15 KHz

The SNR of the received signal can be defined as

$$\text{SNR} = \frac{\mathbb{E}\left\{|y[n]|^2\right\}}{\sigma_v^2}. \tag{40}$$

In order to provide a fair SER comparison between PSAM and our proposed PPST, an effective SNR can be defined when assessing the performance of data transmission, in order to take into account that PSAM and ST do not imply the same data-rate since they are using different pilot overheads. The effective SNR can be expressed as

$$\text{SNR}_d = \mu_e^{-1}\text{SNR}, \tag{41}$$

where μ_e is the efficiency of the system due to the use of pilot symbols, and the sub-index e is a token that can be either PSAM or PPST. For the case of PPST, $\mu_{\text{PPST}} = 1$, while for PSAM, $\mu_{\text{PSAM}} = 13/14$ and $\mu_{\text{PSAM}} = 12/14$ for 5G-C1-1 and 5G-C1-2, respectively. Note that the effective SNR is only used when SER is compared in Figs. 9a-9c.

A. Mean squared error (MSE) performance

Figure 8 shows the MSE of the channel estimation at pilot symbols positions (before interpolation (BI)), and the whole time-frequency resource grid (after interpolation (AI)). Note that a cubic interpolation method is chosen for both time and frequency dimensions. Moreover, the analytical results obtained from (29) are included to check their accuracy.

Figure 8a shows a comparison in terms of MSE of the estimated channel between our proposed PPST technique and PSAM for a channel with a delay spread of 39 ns, $f_d = 35$ Hz and $Q = 38$. Our proposal significantly outperforms PSAM for all values of SNR when $B = 4$, and for low and moderate values of SNR when $B = 1$. This verifies that averaging in both time and frequency domains is capable of reducing the effect of noise and interference effects. Note that the averaging in time domain can be also implemented in PSAM. However, it requires the additional transmission of more pilot symbols for a given slot, and hence, the data-rate is decreased even further, decreasing the effective SNR and worsening the error performance of data transmission, as shown in Sub-section V-B. The saturation of the MSE for our proposal at high SNR is due to the presence of the residual interference introduced by data symbols. Nevertheless, its value is low enough to allow data detection, as illustrated later. On the other hand, the MSE of PSAM is mainly determined by the noise power (σ_v^2).

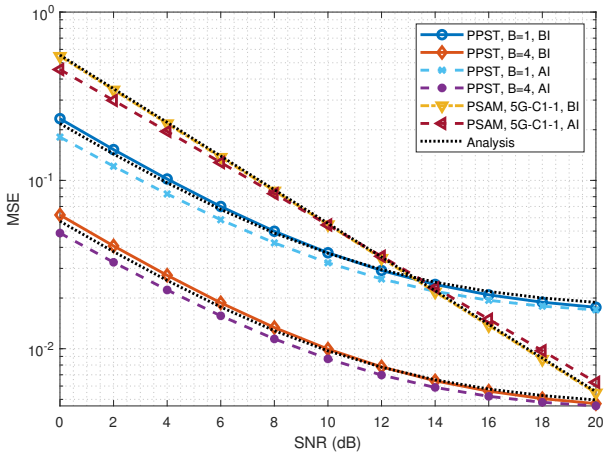

(a) Delay spread of 39 ns, f_d = 35 Hz and Q = 38.

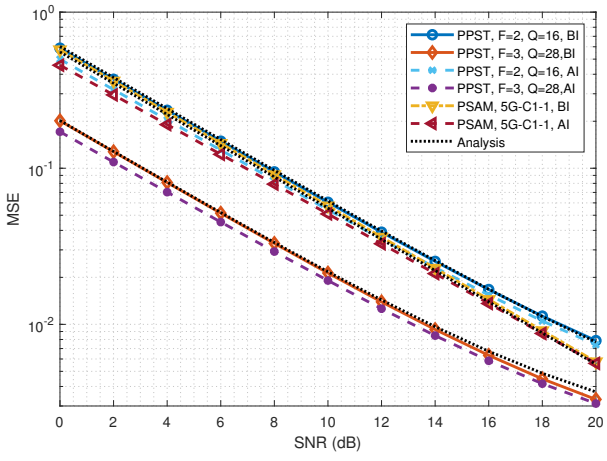

(b) Delay spread of 634 ns, f_d = 35 Hz and B = 6.

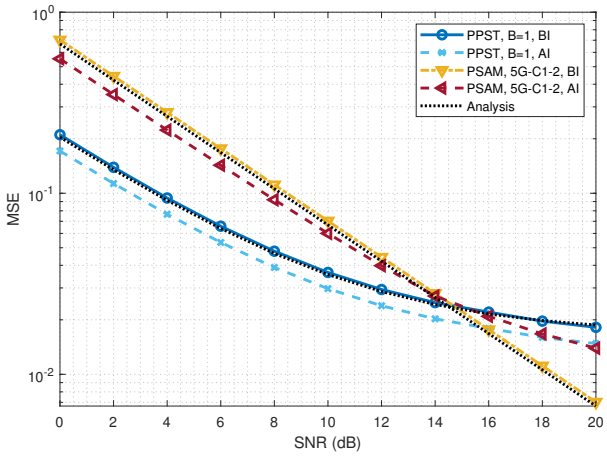

(c) Delay spread of 39 ns, f_d = 300 Hz and Q = 38

Fig. 8. MSE comparison of the estimated channel.

In Fig. 8b, comparison in terms of MSE of the estimated channel between PPST and PSAM for a delay spread of 634 ns, f_d = 35 Hz and B = 6 is provided. It can be observed that for both the BI and AI cases, our proposal still outperforms PSAM for all values of SNR. When the channel is strongly frequency-selective, more pilot symbols must be transmitted in the frequency dimension to capture its variability in this dimension, and hence, not only Q is reduced in order to increase the number of PPST pilot symbols in the frequency domain, but also these pilot symbols must be shifted in the frequency domain from one multi-carrier symbol to the next one, as shown in Fig. 6. It can be seen that the performance for F = 3 is better than for F = 2 due to the fact that the former provides a higher number of channel estimates at different positions in the frequency dimension. However, even though the number or PPST pilots has been increased, the performance of our proposal has worsened as compared to the previous case, especially for low and medium values of SNR, since the delay spread has significantly increased from 39 to 634 ns. For high values of SNR, the saturation of the MSE has been improved for F = 2 given that the averaging factor in the time dimension is increased to N_F = 3.

In Fig. 8c, a comparison in terms of MSE of the estimated channel between our proposal and PSAM for a delay spread of 39 ns, f_d = 300 Hz and Q = 38 is shown. Our proposed scheme, with both BI and AI, significantly outperforms PSAM for low and moderate values of SNR. In addition, for the particular case of high SNR in PSAM, the quality of the estimated channel is significantly degraded due to the Doppler effect, since the channel estimates may be easily outdated if there are not enough pilot symbols in the time dimension. On the contrary, our proposal pours the pilot symbols at the spectrum holes of each CB-FMT symbol, and hence, the channel is frequently updated without impacting the data-rate. Even though both schemes have the same MSE after interpolation, our proposal outperforms PSAM in terms of SER and achievable rate as shown in the following sub-sections.

B. Symbol error rate (SER) performance

In this subsection, the SER performance comparison between PSAM and PPST for QPSK and 16-QAM constellations is illustrated.

In Fig. 9a, a comparison in terms of SER of our proposal and PSAM schemes under the same conditions described in Fig. 8a is provided. It can be seen that the performance for B = 4 is better than for B = 1 due to the fact that an additional averaging in the time domain results in a better channel estimation and consequently, a better SER performance. Moreover, our proposed PPST scheme outperforms PSAM for all values of SNR with a gain of 2.1 dB for the case of QPSK and B = 4 because of the channel estimates are updated more frequently over time in PPST than in PSAM, without sacrificing data-rate. For the particular case of 16-QAM, PPST only significantly outperforms PSAM for medium and high SNR values because the averaging process is even more crucial to reduce the undesirable effects of noise and interference.

In Fig. 9b, a comparison in terms of SER of our proposal and PSAM schemes under the same conditions described in Fig. 8b is shown. It can be observed that the performance with the choice Q = 28 is better than with Q = 16 for any scheme. The reason behind is that higher values of Q provide a better protection since data symbols are spread over a higher number of subcarriers by using the outer bank of

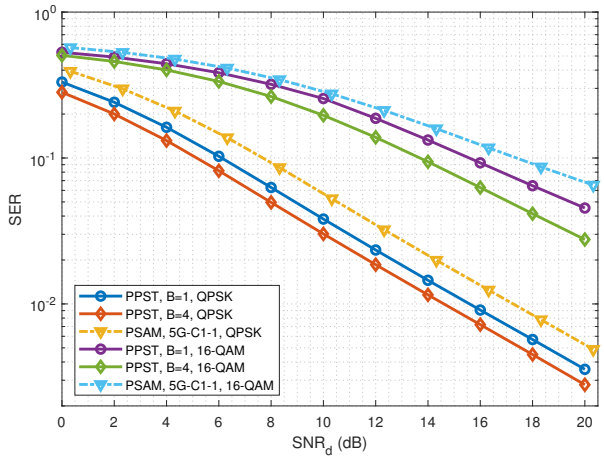

(a) Delay spread of 39 ns, f_d = 35 Hz and Q = 38.

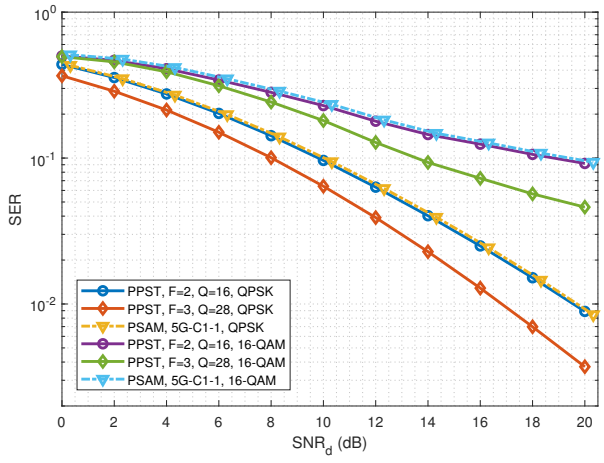

(b) Delay spread of 634 ns and f_d = 35 Hz and B = 6.

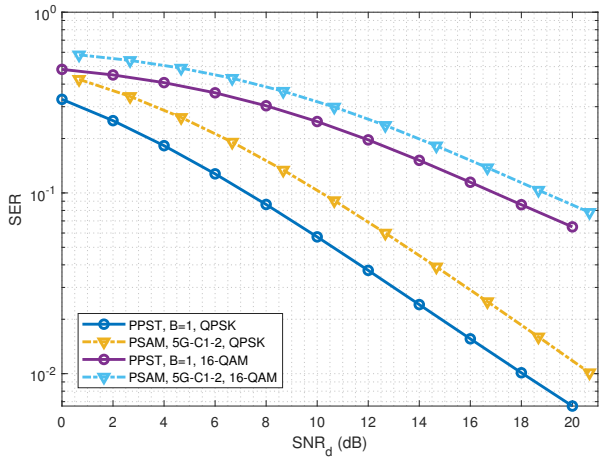

(c) Delay spread of 39 ns, f_d = 300 Hz and Q = 38.

Fig. 9. SER comparison.

DFTs. This makes the system more robust against deep-fading affecting some particular subcarriers which appears in high delay spread channels, as shown in [4], [12]. Moreover, for the particular case of Q = 28, our proposal outperforms PSAM approximately by 1.7 dB for both constellations and medium values of SNR, given that the channel also remains quasi-static during F CB-FMT symbols.

In Fig. 9c, a comparison of SER between PPST and PSAM schemes under the same conditions described in Fig. 8c is provided. Our proposal outperforms PSAM for all values of SNR with a gain of 2.3 dB and 1.6 dB for QPSK and 16-QAM, respectively. This remarkable performance of PPST comes from the fact that the channel is constantly estimated and updated, since the PPST pilot symbols are poured at every multi-carrier symbol. On the contrary, in PSAM, the pilot symbols are only transmitted once for every seven multi-carrier symbols, following the configuration suggested by the standards. Hence, the estimated channel must be reused until the estimaton is updated, what degrades performance in moderate to high mobility scenarios. The fact that PSAM does not work well in fast-varying scenarios has already been reported when OFDM is combined with MIMO [34].

C. Achievable rate performance

In this section, an achievable rate comparison of PSAM and PPST is given. Assuming Gaussian signalling, the achievable rate can be obtained as

$$R = \mu_e \log_2 (1 + \text{SINR}) \text{ [bps/Hz]}, \tag{42}$$

$$\text{SINR} = \frac{1}{\sigma_v^2 + \frac{1}{Q}\mathbb{E}\left\{\sum_{c\in\mathcal{H}_k}\left(|G_t[c]|^2 + \left|W^T[c]\right|^2\right)\text{MSE}_k\right\}}, \tag{43}$$

where the SINR is the signal-to-interference plus noise ratio of the received symbols after the post-processing blocks and $\mathbb{E}\{\bullet\}$ denotes the expected value. The interference term is caused by the channel estimation error and it is obtained following [20], [24]. This mismatch in the estimation process impacts on the computation of the equalizer coefficients ($D[c]$), and hence, degrades the overall performance of the system. In the particular case of PPST, the channel estimation error also generates an additional negative effect on data symbols in the process of pilot subtraction, as detailed in [20]. Furthermore, the resources required to report the pilot pouring and weighted average coefficients are not taken into account, due to the fact that they are negligible when compared to data rate, as it was shown in Section IV.

Figures 10a-10c show the comparison of achievable rates between PPST and PSAM under the conditions described in Figs. 8a-8c, respectively. Again, it is noted that the performance of our proposed PPST is superior when compared to traditional PSAM. Especially, for the particular case of f_d = 300 Hz (Fig. 10c), the performance of PPST is significantly better than the one of PSAM, given that the overhead induced by pilot symbols in PSAM (5G-C1-2) reduces data-rate for highly time-varying channels, as already mentioned in former sub-sections.

VI. Conclusion

In the present work, it was analysed how to efficiently perform channel estimation for CB-FMT. A novel approach referred to as PPST was proposed, which is a generalization of the classical ST technique. Unlike classical ST, it is able to work in a multi-carrier system whose subcarriers are experiencing different values of allocated power.

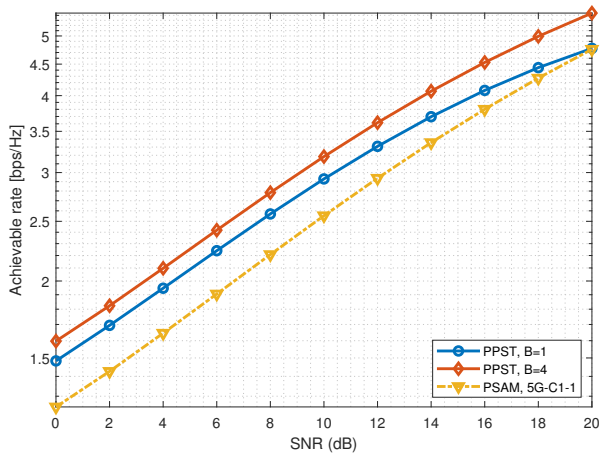

(a) Delay spread of 39 ns, $f_d = 35$ Hz and $Q = 38$.

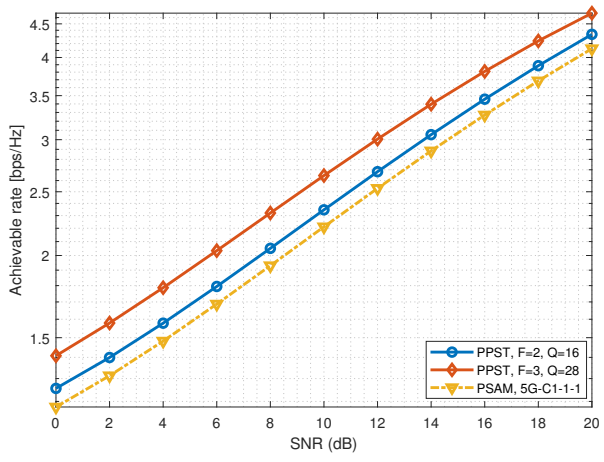

(b) Delay spread of 634 ns and $f_d = 35$ Hz and $B = 6$.

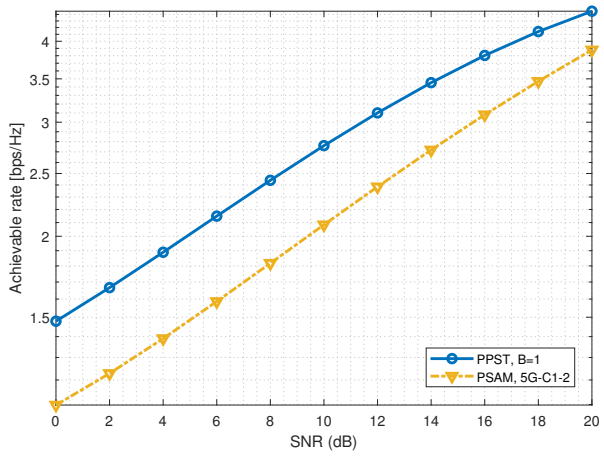

(c) Delay spread of 39 ns, $f_d = 300$ Hz and $Q = 38$

Fig. 10. Achievable rate comparison.

Furthermore, it is capable of avoiding the data-rate reduction penalty that is present when considering traditional PSAM. In this proposal, pilot symbols are allocated and their power is poured over data in a ST fashion, taking advantage of the spectral holes left by the prototype filter in the frequency domain. Besides, at the receiver, an additional weighted average in the frequency dimension is proposed in order to weight each channel estimate, enhancing only those ones which come from pilot symbols with a higher allocated power, and hence, reducing the intrinsic interference produced by data symbols and noise.

The MSE analysis of the channel estimation when applying PPST is provided. The minimization of the MSE allows to obtain the optimal values of pilot pouring and weighted average coefficients. The numerical evaluation of MSE, SER and achievable rate performance in different channel scenarios provided evidence of the superiority of the proposed PPST technique compared to traditional PSAM implemented with CB-FMT, using a pilot pattern given in 5G. Therefore, CB-FMT combined with PPST is a viable alternative to traditional OFDM when spectral confinement and reduced PAPR are important requirements.

Appendix A
Derivation of the MSE of the channel estimation

In this appendix, the details on how to obtain the MSE of the channel estimation at each subcarrier of CB-FMT with PPST are provided.

The estimated channel is modelled as

$$\widehat{H}\left[c\right] = H\left[c\right] + \Delta\left[c\right], \quad 0 \leq c \leq M-1, \tag{44}$$

where $\Delta\left[c\right]$ is the channel estimation error at c-th subcarrier, and according to (22), it is given by

$$\Delta\left[c\right] = \frac{1}{B}\frac{1}{W^T\left[c\right]}\left(H\left[c\right]\sum_{b=0}^{B-1}\frac{X_b\left[c\right]}{X_b^p\left[c\right]} + \sum_{b=0}^{B-1}\frac{V_b\left[c\right]}{X_b^p\left[c\right]}\right), \tag{45}$$
$$0 \leq c \leq M-1.$$

The MSE of the channel estimation at the c-th subcarrier can be obtained as

$$\begin{aligned}\mathrm{MSE}_c = \mathbb{E}\left\{\left|\Delta\left[c\right]\right|^2\right\} = \frac{1}{B^2\left|W^T\left[c\right]\right|^2}\times \\ \times\mathbb{E}\left\{\left|H\left[c\right]\sum_{b=0}^{B-1}\frac{X_b\left[c\right]}{X_b^p\left[c\right]} + \sum_{b=0}^{B-1}\frac{V_b\left[c\right]}{X_b^p\left[c\right]}\right|^2\right\},\end{aligned} \tag{46}$$
$$0 \leq c \leq M-1.$$

Due to the fact that the channel's frequency response $H\left[c\right]$, transmitted symbols $X_b\left[c\right]$ and noise $V_b\left[c\right]$ are uncorrelated random variables, and the power of pilots is normalized to one, (46) can be simplified to

$$\begin{aligned}\mathrm{MSE}_c &= \frac{1}{B^2\left|W^T\left[c\right]\right|^2}\sum_{b=0}^{B-1}\mathbb{E}\left\{\left|X_b\left[c\right]\right|^2\right\} + \mathbb{E}\left\{\left|V_b\left[c\right]\right|^2\right\} \\ &= \frac{\left|G_t\left[c-kQ\right]\right|^2 + \sigma_v^2}{B\left|W^T\left[c\right]\right|^2},\end{aligned} \tag{47}$$
$$kQ \leq c \leq (k+1)Q-1, \quad 0 \leq k \leq K-1,$$

where the squared value of the channel's frequency response $H\left[c\right]$, the power of data symbols $S_{b,k}\left[c\right]$ and the superimposed pilot symbols $X_b^p\left[c\right]$ are normalized to one.

REFERENCES

[1] G. Cherubini, E. Eleftheriou, and S. Olcer, "Filtered multitone modulation for very high-speed digital subscriber lines," *IEEE Journal on Selected Areas in Communications*, vol. 20, no. 5, pp. 1016–1028, June 2002.

[2] T. Hwang, C. Yang, G. Wu, S. Li, and G. Y. Li, "OFDM and its wireless applications: A survey," *IEEE Transactions on Vehicular Technology*, vol. 58, no. 4, pp. 1673–1694, May 2009.

[3] Jun Cai, Xuemin Shen, and J. W. Mark, "Robust channel estimation for OFDM wireless communication systems," *IEEE Transactions on Wireless Communications*, vol. 3, no. 6, pp. 2060–2071, Nov. 2004.

[4] N. Moret and A. M. Tonello, "Design of orthogonal filtered multitone modulation systems and comparison among efficient realizations," *EURASIP Journal on Advances in Signal Processing*, vol. 141865, Feb. 2010.

[5] L. Zhang, P. Xiao, A. Zafar, A. u. Quddus, and R. Tafazolli, "FBMC system: An insight into doubly dispersive channel impact," *IEEE Transactions on Vehicular Technology*, vol. 66, no. 5, pp. 3942–3956, May 2017.

[6] H. Nam, M. Choi, S. Han, C. Kim, S. Choi, and D. Hong, "A new filter-bank multicarrier system with two prototype filters for QAM symbols transmission and reception," *IEEE Transactions on Wireless Communications*, vol. 15, no. 9, pp. 5998–6009, Sep. 2016.

[7] W. Liu, S. Schwarz, M. Rupp, D. Chen, and T. Jiang, "Preamble-based channel estimation for OQAM/FBMC systems with delay diversity," *IEEE Transactions on Wireless Communications*, pp. 1–1, 2020.

[8] X. Chen, L. Wu, Z. Zhang, J. Dang, and J. Wang, "Adaptive modulation and filter configuration in universal filtered multi-carrier systems," *IEEE Transactions on Wireless Communications*, vol. 17, no. 3, pp. 1869–1881, March 2018.

[9] A. F. Almutairi, M. Al-Gharabally, and A. Krishna, "Performance analysis of hybrid peak to average power ratio reduction techniques in 5g ufmc systems," *IEEE Access*, vol. 7, pp. 80 651–80 660, 2019.

[10] D. Zhang, A. Festag, and G. P. Fettweis, "Performance of generalized frequency division multiplexing based physical layer in vehicular communications," *IEEE Transactions on Vehicular Technology*, vol. 66, no. 11, pp. 9809–9824, Nov. 2017.

[11] X. Zhang, Z. Wang, X. Ning, and H. Xie, "On the performance of GFDM assisted NOMA schemes," *IEEE Access*, vol. 8, pp. 88 961–88 968, 2020.

[12] A. M. Tonello and M. Girotto, "Cyclic block filtered multitone modulation," *EURASIP Journal on Advances in Signal Processing*, vol. 109, July 2014.

[13] M. Girotto and A. M. Tonello, "Orthogonal design of cyclic block filtered multitone modulation," *IEEE Transactions on Communications*, vol. 64, no. 11, pp. 4667–4679, Nov. 2016.

[14] *Evolved Universal Terrestrial Radio Access (E-UTRA); Physical channels and modulation*, 3GPP Std. 36.211, 2017.

[15] *NR; Physical channels and modulation (Release 16)*, 3GPP Std. 38.211, 2020.

[16] W. Yan, X. Yuan, Z. He, and X. Kuai, "Passive beamforming and information transfer design for reconfigurable intelligent surfaces aided multiuser mimo systems," *IEEE Journal on Selected Areas in Communications*, pp. 1–1, 2020.

[17] T. K. Vu, M. Bennis, M. Debbah, and M. Latva-Aho, "Joint path selection and rate allocation framework for 5G self-backhauled mm-wave networks," *IEEE Transactions on Wireless Communications*, vol. 18, no. 4, pp. 2431–2445, April 2019.

[18] M. K. Tsatsanis and Zhengyuan Xu, "Pilot symbol assisted modulation in frequency selective fading wireless channels," *IEEE Transactions on Signal Processing*, vol. 48, no. 8, pp. 2353–2365, Aug. 2000.

[19] J. Lin, "Least-squares channel estimation for mobile OFDM communication on time-varying frequency-selective fading channels," *IEEE Transactions on Vehicular Technology*, vol. 57, no. 6, pp. 3538–3550, Nov. 2008.

[20] W. Huang, C. Li, and H. Li, "On the power allocation and system capacity of OFDM systems using superimposed training schemes," *IEEE Transactions on Vehicular Technology*, vol. 58, no. 4, pp. 1731–1740, May 2009.

[21] S. He, J. K. Tugnait, and X. Meng, "On superimposed training for MIMO channel estimation and symbol detection," *IEEE Transactions on Signal Processing*, vol. 55, no. 6, pp. 3007–3021, June 2007.

[22] X. Xie, M. Peng, F. Gao, and W. Wang, "Superimposed training based channel estimation for uplink multiple access relay networks," *IEEE Transactions on Wireless Communications*, vol. 14, no. 8, pp. 4439–4453, Aug. 2015.

[23] K. Chen-Hu, J. C. Estrada-Jiménez, M. J. Fernández-Getino García, and A. G. Armada, "Superimposed training for channel estimation in FBMC-OQAM," in *2017 IEEE 86th Vehicular Technology Conference (VTC-Fall)*, Sep. 2017, pp. 1–5.

[24] J. C. Estrada-Jiménez, K. Chen-Hu, M. J. Fernández-Getino García, and A. García Armada, "Power allocation and capacity analysis for FBMC-OQAM with superimposed training," *IEEE Access*, vol. 7, pp. 46 968–46 976, 2019.

[25] J. C. Estrada-Jiménez and M. J. Fernández-Getino García, "Partial-data superimposed training with data precoding for OFDM systems," *IEEE Transactions on Broadcasting*, vol. 65, no. 2, pp. 234–244, June 2019.

[26] G. Arfken, *Mathematical Methods for Physicists*, 3rd ed. San Diego: Academic Press, Inc., 1985.

[27] A. Hedayat and A. Nosratinia, "Outage and diversity of linear receivers in flat-fading MIMO channels," *IEEE Transactions on Signal Processing*, vol. 55, no. 12, pp. 5868–5873, Dec. 2007.

[28] Jeongho Park, Jihyung Kim, Myonghee Park, Kyunbyoung Ko, Changeon Kang, and Daesik Hong, "Performance analysis of channel estimation for OFDM systems with residual timing offset," *IEEE Transactions on Wireless Communications*, vol. 5, no. 7, pp. 1622–1625, July 2006.

[29] P. Tsai and T. Chiueh, "Adaptive raised-cosine channel interpolation for pilot-aided OFDM systems," *IEEE Transactions on Wireless Communications*, vol. 8, no. 2, pp. 1028–1037, Feb. 2009.

[30] S. Boyd and L. Vandenberghe, *Convex Optimization*. USA: Cambridge University Press, 2004.

[31] C. Clapham and J. Nicholson, *The Concise Oxford Dictionary of Mathematics*, 4th ed. Oxford University Press, 2009.

[32] *Study on channel model for frequencies from 0.5 to 100 GHz (Release 15)*, 3GPP Std. 38.901, 2018.

[33] Won-Gyu Song and Jong-Tae Lim, "Pilot-symbol aided channel estimation for OFDM with fast-fading channels," *IEEE Transactions on Broadcasting*, vol. 49, no. 4, pp. 398–402, 2003.

[34] M. J. López-Morales, K. Chen-Hu, and A. García-Armada, "Differential data-aided channel estimation for up-link massive SIMO-OFDM," *IEEE Open Journal of the Communications Society*, vol. 1, pp. 976–989, 2020.

Kun Chen-Hu (S'16-GS'20-M'21) received his Ph.D. degree in Multimedia and Communications in 2019 from Universidad Carlos III de Madrid (Spain). Currently, he is a post-doctoral researcher in the same institution. He was awarded by UC3M in 2019 recognizing his outstanding professional career after graduation. He visited Eurecom (France) and Vodafone Chair TU Dresden (Germany), both as guest researcher. He also participated in different research projects in collaboration with several top companies in the area of mobile communications. He is the Web Chair for Globecom 2021, Madid (Spain), and online content editor for IEEE ComSoc. His research interests are related to signal processing techniques, such as waveforms design, reconfigurable intelligent surfaces, non-coherent massive MIMO and channel estimation.

M. Julia Fernández-Getino García (S'99 - AM'02 - M'03) received the M. Eng. and Ph.D. degrees in telecommunication engineering from the Polytechnic University of Madrid, Spain, in 1996 and 2001, respectively. She is currently with the Department of Signal Theory and Communications, Carlos III University of Madrid, Spain, as an Associate Professor. From 1996 to 2001, she held a research position with the Department of Signals, Systems and Radiocommunications, Polytechnic University of Madrid. She visited Bell Laboratories, Murray Hill, NJ, USA, in 1998; visited Lund University, Sweden, during two periods in 1999 and 2000; visited Politecnico di Torino, Italy, in 2003 and 2004; and visited Aveiro University, Portugal, in 2009 and 2010. Her research interests include multicarrier communications, coding and signal processing for wireless systems.

She received the best "Master Thesis" and "Ph.D. Thesis" awards from the Professional Association of Telecommunication Engineers of Spain in 1998 and 2003, respectively; the "Student Paper Award" at the IEEE International Symposium on Personal, Indoor and Mobile Radio Communications (PIMRC) in 1999; the "Certificate of Appreciation" at the IEEE Vehicular Technology Conference (VTC) in 2000; the "Ph.D. Extraordinary Award" from the Polytechnic University of Madrid in 2004; the "Juan de la Cierva National Award" from AENA Foundation in 2004; and the "Excellence Award" from Carlos III University of Madrid in 2012 for her research career.

Andrea M. Tonello (M'00-SM'12) received the Laurea degree (summa cum laude) in electrical engineering and the Doctor of Research degree in electronics and telecommunications from the University of Padova, Padua, Italy, in 1996 and 2002, respectively. From 1997 to 2002, he was with Bell Labs-Lucent Technologies, Whippany, NJ, USA, first as a Member of the Technical Staff. He was then promoted to Technical Manager and appointed as the Managing Director of the Bell Labs, Italy Division. In 2003, he joined the University of Udine, Udine, Italy, where he became an Aggregate Professor, in 2005 and an Associate Professor, in 2014. He is currently a Professor with the Chair of Embedded Communication Systems, University of Klagenfurt, Klagenfurt, Austria. He received several awards, including the Bell Labs Recognition of Excellence Award (1999), the Distinguished Visiting Fellowship from the Royal Academy of Engineering, U.K. (2010), the IEEE Distinguished Lecturer Award from VTS (2011-15) and from COMSOC (2018-19), the Italian Full Professor Habilitation (2013), the Chair of Excellence from Carlos III Universidad, Madrid (2019-20). He was also a co-recipient of nine best paper awards. He serves/ed as associate editor of several journals, including IEEE TVT, IEEE TCOM, IEEE ACCESS, and IET Smart Grid. He was the general chair or TPC co-chair of several conferences. He was the chair of the IEEE COMSOC Technical Committee (TC) on Power Line Communications (2014-18) and he is currently the Chair of the TC on Smart Grid Communications. He also serves as Director of Industry Outreach of IEEE COMSOC for the term 2019-20.

Ana García Armada (S'96-A'98-M'00-SM'08) received the Ph.D. degree in electrical engineering from the Polytechnical University of Madrid in February 1998. She is currently a Professor at Universidad Carlos III de Madrid, Spain. She is leading the Communications Research Group at this university. She has participated in more than 30 national and 10 international research projects as well as 20 contracts with the industry. Her research has resulted in 9 book chapters, and more than 150 publications in prestigious international journals and conferences, as well as 5 patents. She has also contributed to standardization organizations (ITU, ETSI) and is a member of the European 5G PPP Group of Experts, as well as the Spanish representative in the committee of the ESA Joint Board on Communication Satellite Programs 5G Advisory Committee (5JAC). She has been Editor (2016–2019, Exemplary Editor Award 2017 and 2018) and Area Editor (2019-2020, Exemplary Editor Award 2020) of IEEE Communication Letters. She is Editor of IEEE Transactions on Communications since 2019, Area Editor of IEEE Open Journal of the Communications Society since 2019, Editor of the ITU Journal on Future and Evolving Technologies and is a regular member of the technical program committees of the most relevant international conferences in his field. She has formed / is part of the organizing committee of the IEEE Globecom 2019 and 2021 (General Chair), IEEE Vehicular Technology Conference Spring 2018, 2019 and Fall 2018, IEEE 5G Summit 2017, among others. She is Secretary of the IEEE ComSoc Signal Processing and Computing for Communications Committee, has been Secretary and Chair of the IEEE ComSoc Women in Communications Engineering Standing Committee. Since January 2020 she is Director of Online Content of the IEEE Communications Society. She has received the Award of Excellence from the Social Council and the Award for Best Teaching Practices from Universidad Carlos II de Madrid, as well as the third place Bell Labs Prize 2014, the Outstanding Service Award 2019 from the SPCE committee of the IEEE Communications Society and the Outstanding Service Award 2020 from the Women in Communications Engineering (WICE) standing committee.